Efficient Sb_2Se_3/CdS Planar Heterojunction Solar Cells in Substrate Configuration with (hk0) Oriented Sb_2Se_3 Thin Films

Kunal J. Tiwari[1,2#], Markus Neuschitzer[1], Moises Espíndola[1], Yudania Sanchez[1], Zacharie Jehl[1], Pedro Vidal[1], Edgardo Saucedo[1] and Piraviperumal Malar[2]

[1]Catalonia Institute for Energy Research (IREC), Sant Adrià de Besòs (Barcelona), Barcelona, 08930, Spain

[2] SRM Research Institute and Department of Physics & Nanotechnology, SRM Institute of Science and Technology, Kattankulathur Chennai, Tamilnadu, 603 203 India

Abstract

Antimony selenide (Sb_2Se_3) based solar cell technology has experienced rapid development with demonstrated cell efficiency reaching~ 9.2% for devices with substrate configuration, hence necessitating more intense research investigation for further progress. Though the effect of crystallographic orientation in this non-cubic material on device performance is now well understood, the influence of composition and intrinsic defects remains debatable. In this work we describe the fabrication and device characteristics of Sb_2Se_3 solar cells designed in the substrate configuration of (SLG/Mo/Sb_2Se_3/CdS/i-ZnO+ITO). Notably, Sb_2Se_3 absorber layers with predominant (hk0) orientation were deposited in a single step by e-beam evaporation of pre synthesized bulk source material. As grown precursor Sb_2Se_3 thin films were subjected to reactive thermal annealing (RTA) treatment in the presence of Se source at different temperatures for enhancing their crystalline quality and balancing their stoichiometry. Analysis of the completed solar cells indicated improved efficiencies post RTA process, with the best performing devices exhibiting a power conversion efficiency (η) of ~ 4.34% for an absorber annealed at a temperature of 350 °C. The improved efficiency is ascribed to the observed changes in chemical composition of the absorber layer and the possible formation of related beneficial antisite defects.

Key words: Antimony Selenide; Solar Cells; Substrate Configuration; E-beam evaporation.

#Corresponding Author

Introduction:

Recently, binary chalcogenide semiconductors such as Sn(S,Se)[1,2], $Sb_2(S/Se)_3$[3,4], $Bi_2(S/Se)_3$[5] etc., have garnered substantial attention as a potential absorber layer material in thin film solar cell (TFSC)[6] applications. TFSC incorporating Sb_2Se_3 as a p-type light absorber has exhibited promising efficiency of ~ 9.2% in a relatively very short span of time[7]. Its simple binary composition, relatively low processing temperature, suitable yet tunable optical band gap (E_g = 1-1.3 eV) and high absorption coefficient (>10^5 cm^{-1}) are the prime merits of Sb_2Se_3 leading to a growing interest and exploratory research on this material[8].

Sb_2Se_3 crystallizes in layered orthorhombic crystal structure showing anisotropic charge transport properties[9]. Tang et al. have reported that the control over the crystallographic orientation is of prime importance in Sb_2Se_3 to obtain solar cells with high power conversion efficiencies. This was realized through controlling the thin film growth conditions, most prominently the temperature[4,10,11]. Various studies reported that Sb_2Se_3 thin films with preferred crystallographic orientation along the (hk1) specifically (221) direction has resulted in devices with higher efficiencies[9,12–17]. Prime reason for better performance was identified as the ease of charge transport through the ribbons oriented along (hk1) crystal plane perpendicular to the substrate and benign grain boundaries in this material[18].

Major progresses have recently been made on the Sb_2Se_3 solar cells with superstrate configuration, and the current record efficiency stands at 7.04%[19]. In contrast, Sb_2Se_3 solar cells grown from a substrate configuration remain surprisingly overlooked, although a certified record efficiency value of ~ 9.2% for nano structured solar cells in substrate configuration was recently reported[7]. In the mentioned report, an Sb_2Se_3 nanorod array was fabricated and the effect of interfacial TiO_2

layer on the properties of the solar cell devices was studied. For the thin film solar cell with planar heterojunction in substrate configuration, a record efficiency of 6.5% has been reported with the $Cd_{0.75}Zn_{0.25}S$ buffer layer [20]. In the discussed work, Sb_2Se_3 absorber layer with (221) orientation was prepared on Mo coated substrates by closed space sublimation method. In another work[16], the authors reported the effect of back contact selenization on the efficiency of solar cells in substrate configuration. A post selenization process of the back contact led to the enhancement in (221) texture of absorber resulting in the solar cells with efficiency of 4.25%.

Though the influence of the crystallographic orientation of polycrystalline Sb_2Se_3 thin films on performance of devices is now well understood, very few research studies were performed to elaborate on the effect of the electrically active defects[13,21–24]. Liu et al.[21] performed a detailed study on the formation of intrinsic defects in thermally evaporated Sb_2Se_3 thin films under different film growth conditions. It was observed that Se-poor thin films led to the formation of donor defects Se vacancies (V_{se}). Whereas under Se rich film growth conditions, the prospect of formation of acceptor antisite defects like Se_{Sb} is highly expected. By modifying the defect concentration, solar cells with an efficiency of 5.7% were obtained in their work. Hence control over the stoichiometry in thin film is deemed of equal importance to the crystallographic orientation. Here we have tried to modify the Se concentration in the Sb_2Se_3 absorber layer and studied the opto-electronic properties of the completed solar cells.

In the present work, Sb_2Se_3 heterojunction solar cells were completed in substrate configuration using a post deposition heat treatment of the absorber deposited through e-beam evaporation in single step. Chemical composition of the as grown Sb_2Se_3 precursor film has been altered through RTA under Se atmosphere at different temperatures. The effect of changes in the composition was discussed in regard to the performance of the resulting solar cell devices. Though the thin films

were (hk0) oriented, comparable device efficiency was still obtained for the completed solar cell devices, which we attributed to the changes in the doping concentration of the absorber as well as passivation of the native defects in absorber. Also, the effect of variation in stoichiometry with respect to the annealing temperature clearly reflected in the doping concentration of Sb_2Se_3 absorber layer obtained from room temperature C-V measurement of solar cells. Those results are consistent with the observed J-V behavior of the solar cells under illumination. As far as literature is concerned, this work is to the best of our knowledge the first one to report Sb_2Se_3 solar cells with (hk0) oriented absorber exhibiting power conversion efficiency close to the one reported for the standard (hk1) oriented films (Table S1). In this regards, this report presents novel results highlighting the importance of Se concentration in the absorber and brings insights on its impact on the device performance.

Experimental Methods:

Device Fabrication:

Sb_2Se_3 precursor films were deposited on the molybdenum (Mo) coated glass substrates by e-beam evaporation of mechano-chemically synthesized bulk source material. DC Sputter deposited Mo with average thickness between ~ 750-800 nm was used as the back contact. The details of thin film deposition process have been reported elsewhere [25]. Mechano -chemically synthesized bulk source material was placed in a graphite crucible and used as evaporation source. Careful optimizations of the absorber thickness, growth temperature as well as annealing temperature were done to obtain the functional solar cell devices. In this study Sb_2Se_3 thin films were deposited at the optimized substrate temperature of ~ 320 °C. The substrate was held static during the deposition process. Post deposition RTA process was performed at three different temperatures namely ~ 320, ~ 350 and ~ 380°C. For annealing, the as-deposited precursor films were loaded in

the graphite box with 20 mg Se powder. The box was inserted in a three-zone tubular furnace ensuring uniform heating. The temperature was increased at a rate of 20 °C/min and maintained at a dwelling time of 30 minutes. Heat treatment was performed under Ar atmosphere maintaining the total pressure at 800 mbar over the entire heating process. Subsequently the furnace was allowed to cool down naturally to room temperature before extracting the samples for further characterization and device completion. Solar cell devices were completed in the substrate configuration glass/Mo/Sb_2Se_3/CdS/i-ZnO/ITO. N-type CdS buffer layer was deposited through chemical bath deposition. Window layers, namely i-ZnO and ITO thin films, were deposited through the pulsed DC-sputtering technique. Details of the experimental conditions for other processes has been described in detail elsewhere[26]. No anti reflection coating was used in the completed devices. Solar cells with an area of 0.087 cm^2 were isolated using the micro diamond scriber MR200OEG (OEG Gesellschaft für Optik, Elektronik & GerätetechnikmbH, Frankfurt, Germany) for electrical characterization of the devices.

Material Characterization:

As grown and annealed Sb_2Se_3 thin films were characterized through the X-ray diffraction (XRD) technique for structure and phase confirmation. XRD measurements were performed on the Bruker D8 Advance XRD tool in the classical Bragg Brentano geometry using Cu Kα line (λ~1.58 Å) source. Chemical composition of the as grown and annealed thin film samples were determined through the X-ray fluorescence (XRF) spectroscopy. XRF measurements were performed using Fischerscope model XDV instrument. Microstructure and thickness of the as grown and annealed thin film sample were inferred through the cross sectional SEM images. SEM imaging was performed on the Zeiss series Auriga electron microscope with the accelerating voltage of 5 kV under ambient conditions.

Device Characterization:

Current density vs. voltage (J-V) characteristics of the devices were studied under dark condition and AM 1.5 illuminated conditions using an ABET class AAA solar simulator. All the measurements were performed at room temperature. External quantum efficiency (EQE) spectra of the solar cells was recorded using a Bentham PV instrument. Before measurement, the system was calibrated with standard Si and Ge photodiodes. Room temperature capacitance vs. voltage (C-V) measurements were performed on the completed solar cell devices using Agilent E4980A LCR meter. Doping density as well as the width of the space charge region was determined from the capacitance values calculated in the parallel circuit model.

Results and Discussion:

Structural Characterization:

Normalized XRD patterns for the as grown absorber film and thin film annealed at different temperatures are shown in fig.1(a). Sharp well resolved peaks in the recorded XRD pattern confirmed polycrystalline nature of the as grown and annealed thin film samples.

The lattice planes are indexed with reference to ICDD file no. 01-089-0821 confirming formation of orthorhombic Sb_2Se_3 with space group *Pbnm*. As the measurement was performed under conventional Bragg Brentano geometry, the maximum intensity peak observed at $2\theta = 40.1°$ was ascribed to the Mo substrate for all the samples. Except for that specific peak, all other diffraction peaks observed were due to Sb_2Se_3 phase with the dominant peak corresponding to (120) crystallographic plane.

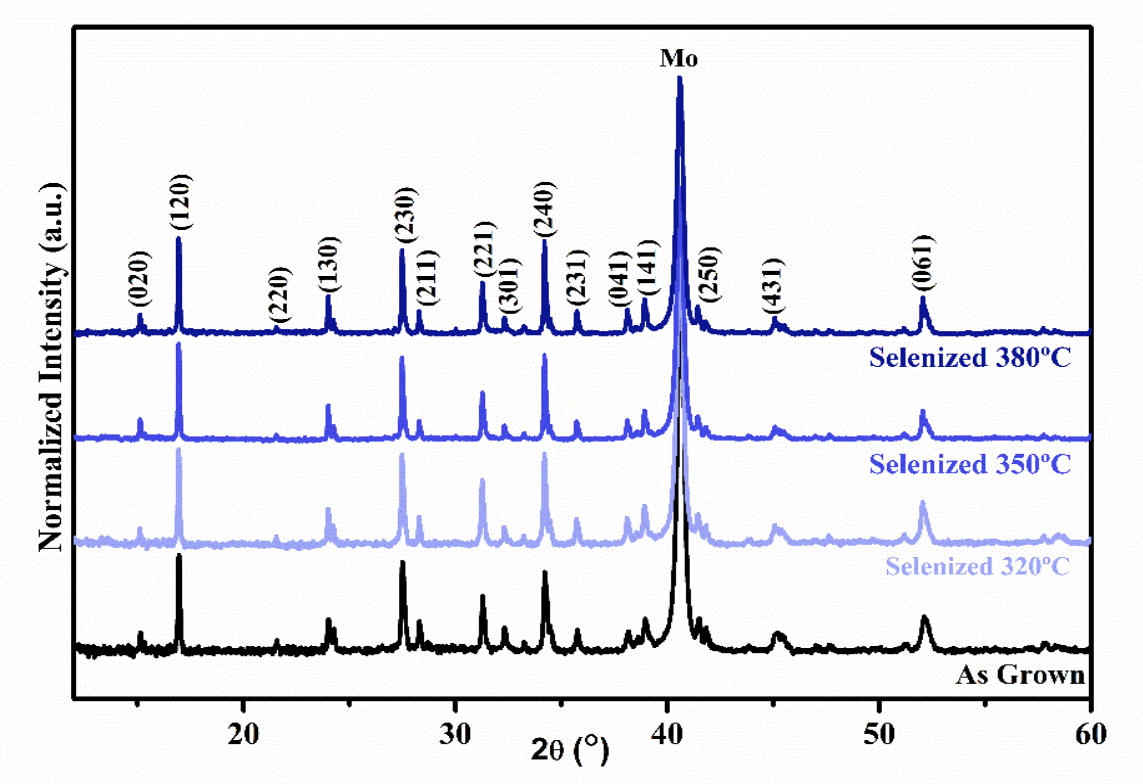

Fig.2. XRD diffractogram for as grown and annealed Sb_2Se_3 thin films.

The analysis of the XRD results confirmed the growth of the films with a favored orientation along the (hk0) crystallographic plane. The presence of relatively less intense peaks corresponding to the planes with (hk1) orientation namely (221), (211) etc. was also confirmed. Interestingly, no significant changes were observed in the XRD pattern for the as grown and annealed thin film samples. This observation is indicative, that reactive thermal annealing has only lead to the changes in the stoichiometry and it has negligible impact on the crystallographic orientation of the Sb_2Se_3 thin films.

Cross sectional SEM micrographs for the as grown and annealed thin film samples are shown in the figure 2. Thin film with a uniform thickness and densely packed grains are observed and confirm the good crystallinity of the films, consistently with the previously discussed XRD results.

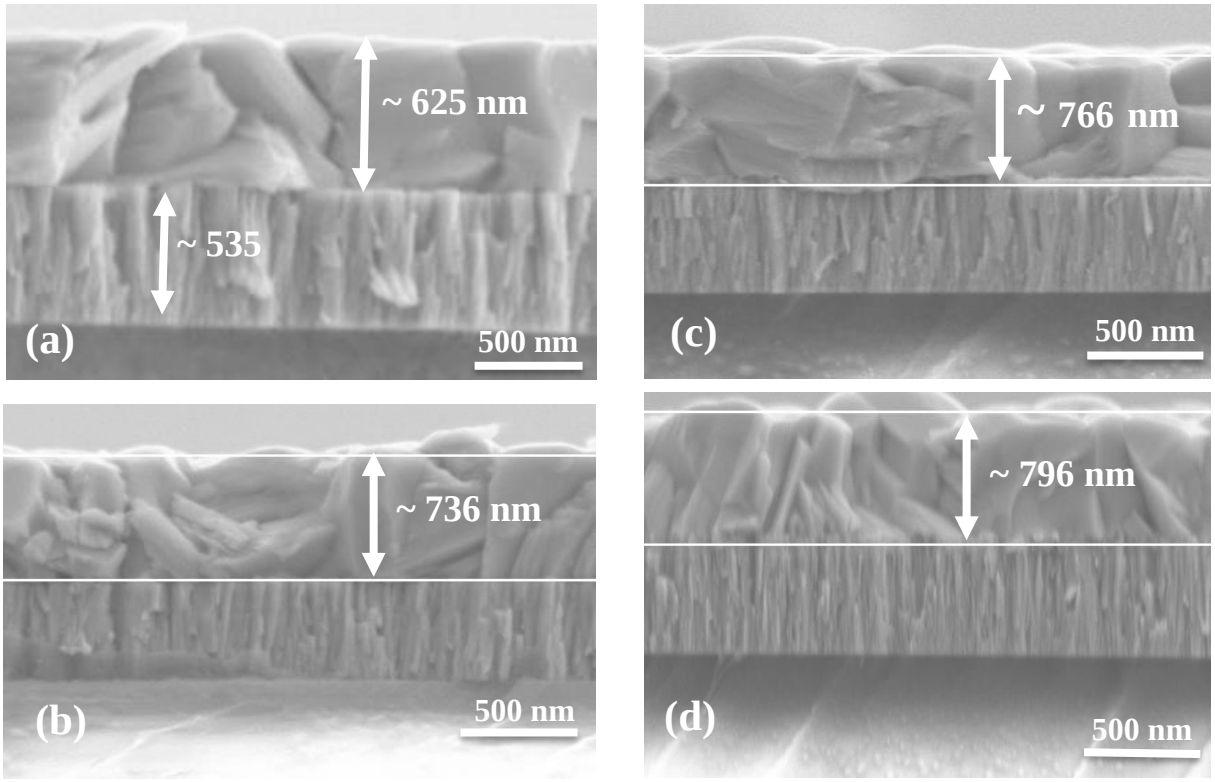

Fig.2. SEM micrograpg for as grown and annealed Sb_2Se_3 thin films (a) as grown (b) annealed at 320 °C (c) annealed at 350 °C (d) annealed at 380 °C

An improvement in the apparent surface smoothness was also observed with the increase in the selenization temperature, as evident from the cross sectioned micro graph; however, this observation would need confirmation through a proper surface analysis using atomic force microscopy (AFM). It is worth noting that a similar reduced surface roughness as a result of post selenization has been reported by earlier studies[14,21]. Thickness values of the as grown and selenized absorber layers were determined from the cross section SEM micrographs and found to be in the range of 700-800 nm.

Compositional Analysis:

The chemical composition of the as grown and selenized Sb_2Se_3 thin films was analyzed through XRF spectroscopy measurement. The results of the XRF measurement indicated an increase in the

Se concentration post selenization of the as grown absorber layer. A linear increment of Se amount in the absorber with increasing RTA temperature was observed for the as grown absrober, represented in a graphic fig. S1. The observed atomic percentage values for the Sb and Se in the as grown and selenized thin film samples are presented in table 1. It is evident from the table that as grown thin film sample had a Se poor and slighlty Sb rich chemical composition. As thin films in this study were grown by high energy e-beam PVD method, a substantial Se loss is highly expected due to the high vapor pressure of this element compared to Sb_2Se_3 and Sb. Hence heat treatment under Se atmosphere has also been suggested in the previous studies as a solution for compensating Se loss during evaporation [14,21,23]. Thin films annealed at a temperature of 320 °C showed atomic percentage values (Sb ~ 39.75% and Se ~ 60.25) close to the ideal stoichiometric ratio of 2:3. Whereas films annealed at a temperature of 350 and 380 °C show in contrast highly Se rich and Sb poor compositions. This trend indicates an increased incorporation of Se with the RTA temperature. Though no significant improvement in the crystalline quality were detected, changes in the crystallographic orientation and no addtional secondary phases are observed in the XRD analysis post annealing of the samples. In compoud semiconductors, the intrinsic defect density is closely linked to the chemical composition through the formation of vacancies or antisite elements. Hence, a change in the sotichiometry of the films as observed here is expected to yield modifications in the defect, and thus in the electrical properties of the final devices. The performances of the completed solar cell devices were evaluated and the results are discussed in the following section. Furthmore, to have a deeper insight is brought by C-V measurements were performed on the completed solar cell devices, and will be discussed further in the manuscript.

Elements (Atomic %)	Substrate Temperature 320 °C			
	As Grown	Annealing Temperature		
		320°C	350°C	380°C
Sb (%)	41.36	39.75	37.83	36.26
Se (%)	58.64	60.25	62.16	63.73

Table 1. Composition of Sb_2Se_3 absorber determined through XRF

Current Density (J) vs. Voltage (V) Studies

J-V curves for the solar cell were obtained under the dark as well as under illumination in AM 1.5 conditions and are shown in the fig. 2. A representative cross section SEM micrograph of the completed solar cell with different layers is also presented as inset to the figure. Relevant solar cell performance parameters values obtained after the measurement are tabulated in the table 2 along with the other diode parameters extracted from fitting the dark J-V curves using a single diode model. The fitted JV curves under dark condition are shown in the fig. S2 (supplementary file). The analysis of the J-V curves indicated that annealing temperatures in the range of 320-350 °C led to Sb_2Se_3 solar cell devices with the highest efficiencies. A power conversion efficiency of ~ 4.24% was obtained for the cells completed with the absorber annealed at a temperature of 320 °C. The device showed a J_{sc} value of ~ 22 mA/cm^2, V_{oc} ~ 371 mV with FF of 51%. While the efficiency remains almost unchanged at 350C, from 4.24 to 4.34%, a substantial improvement in the fill factor value from 51% to 57% and an increase in V_{oc} from 371 to 386 mV is observed. The reduced current counterbalances these parameters, which will be explained in the following paragraph.

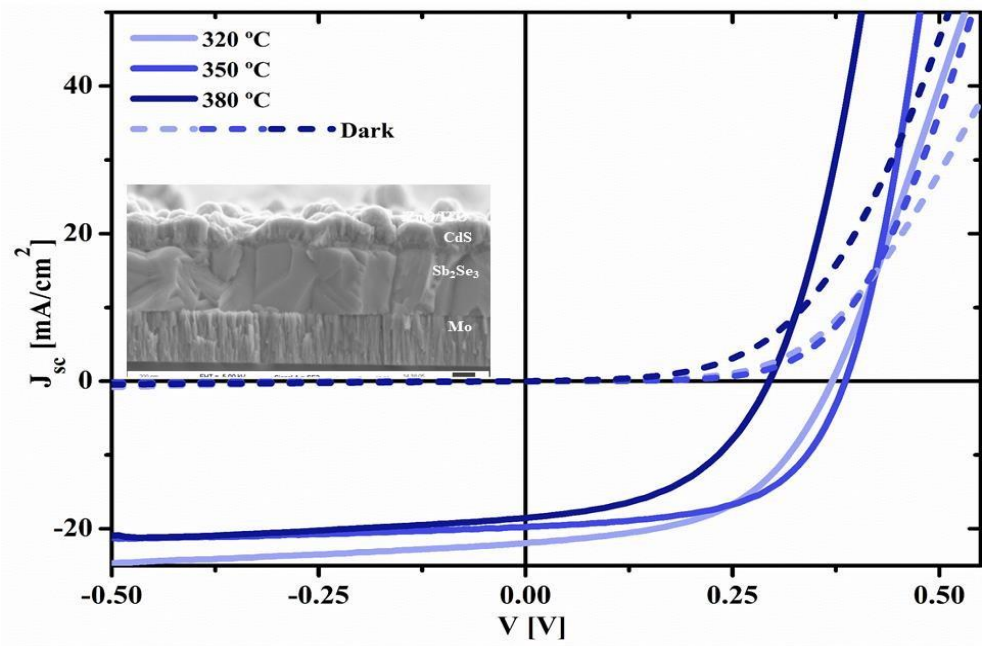

Fig. 2 J-V characteristics of the Sb_2Se_3 solar cells fabricated using films grown at 320 °C and annealed at various substrate temperature. Inset shows the cross sectional SEM micrograph of completed solar cell device.

Experiments' reproducibility was assessed by measuring close to 15 individual solar cell devices for each annealing temperature. The statistical distribution of different device parameters is presented in the form of the box plot in fig. 3. The values of V_{oc} and fill factor for best performing solar cells in this work is comparable with the values mentioned in literature[16]. To discuss the device physics, J-V curves recorded under dark condition were fitted using single diode model to extract the values of series resistance (R_s), shunt resistance (R_{sh}), reverse saturation current density (J_0) and diode ideality factor (A). Significant changes in diode parameters were also observed for the annealing temperatures of 320 °C and 350 °C. Series resistance value was found to decrease marginally (0.4 to 0.2 $\Omega.cm^2$) whereas an almost 5-fold increase in the R_{sh} value (71.79 to 341.88 $\Omega.cm^2$) was observed for the solar cell devices completed with the absorber annealed at 350 °C.

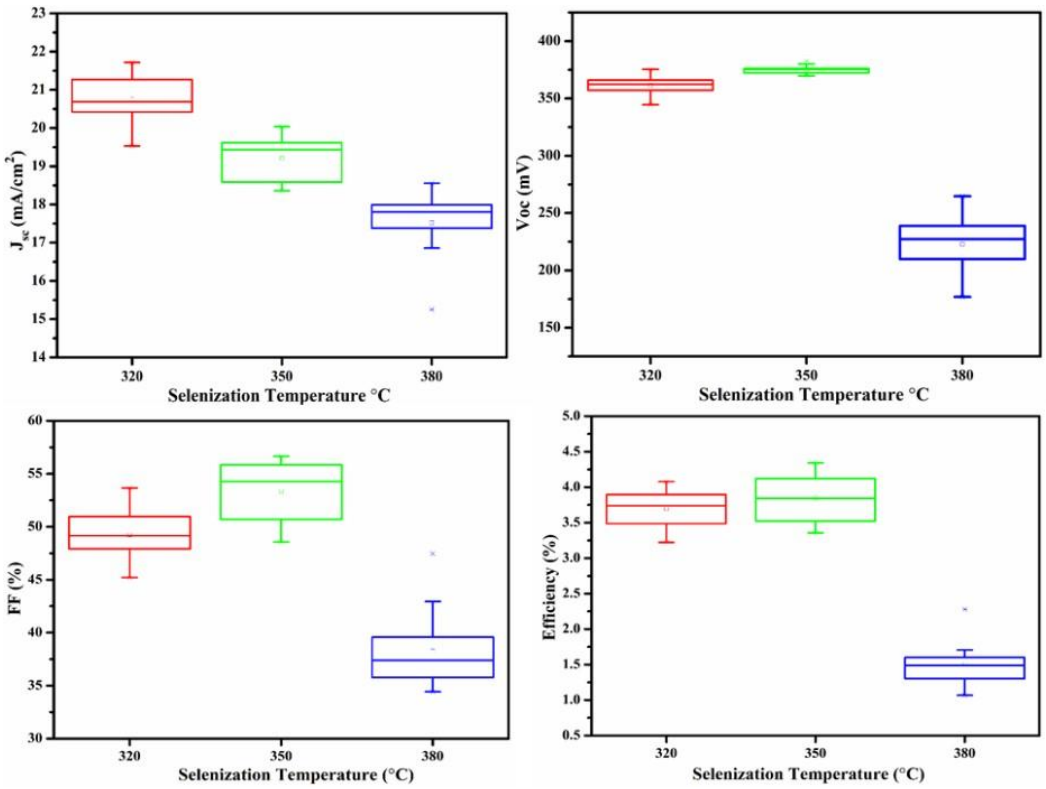

Fig.3 Box plot representing the statistics for different solar cell performance parameters for the Sb_2Se_3 solar cells

A possible reason for the improvement in the observed R_{sh} value could be the passivation of highly conductive grain boundaries in the absorber post reactive thermal annealing, which otherwise act as a bypass to the p-n junction. In addition to the above, a significant drop in the reverse saturation current density with respect to the absorber annealed at the temperature of 320 °C was also observed for the solar cells fabricated with these absorber layers. Diode ideality factor value for these solar cell was found to be ~ 1.4 indicative of the good quality of the junction formation. Improvement in the diode characteristics can be attributed to the changes in the microstructure of the absorber as a result of the selenization process. As mentioned previously, selenization of the absorber layers not only improves the stoichiometry but also possibly reduces the surface roughness, improving the quality of junction (better buffer layer coverage and lower

contact area at the p-n junction) and its diode characteristics. It is worth noticing that though the absorber layer has (hk0) orientation, comparable efficiency reported for (221) oriented Sb_2Se_3 thin films has been obtained [15,16,23]. This indicates that apart from the orientation, stoichiometry as well as the native defects also play important role in defining the performance of solar cells. A compilation of the cell efficiency values reported for Sb_2Se_3 based devices from the literature and the values obtained in this work has been presented in the supplementary information file (table S1) for comparison. A significant drop in efficiency was observed for solar cells fabricated with absorber layer annealed at a temperature of 380 °C, with a device efficiency of ~ 2.3% along a limited fill factor, current and voltage (FF = 47.3%, J_{sc}=18.5 mA/cm^2 and V_{oc}=294 mV). Although the loss in the short circuit current density was relatively small compared to other devices, the drop is much more significant for the V_{oc} and FF. This tends to indicate a degradation in the junction quality. Also, the high ideality factor of this sample tends to indicate that more than one process governs the current density of the cell.

Annealing Temperature	**J_{sc} (mA/cm^2)**	**V_{oc} (mV)**	**FF (%)**	**η (%)**	**R_s (Ω.cm^2)**	**R_{sh} (Ω.cm^2)**	**A_0**	**J_0 (mA/cm^2)**	**SCR width (nm)**	**N_{cv} (cm^{-3})**
320 °C	21.9	371	51.4	4.2	0.4	71.79	1.4	9×10^{-2}	132	2×10^{16}
350 °C	19.8	386	56.7	4.3	0.2	341.88	1.39	3×10^{-2}	92	9×10^{16}
380 °C	18.5	294	47.3	2.6	0.1	87.70	2.7	1.063	67	4×10^{17}

Table 2. Device characteristics of the Sb_2Se_3 solar cells fabricated using the films grown at the substrate temperature of 320 °C and annealed at various temperatures.

EQE Measurements:

To further analyze the behavior of the solar cell devices, external quantum efficiency (EQE) measurements were also carried out under normal as well as reversed biased condition. Solar cell

fabricated using the absorbers annealed at 320 °C showed an EQE value reaching ~ 80% at ~ 580 nm. Afterward, a diminution of the EQE value was observed for the device in the long wavelengths region. The loss in short wavelength region (450-500 nm) can be accounted for the absorption in the top CdS layer. Quantum efficiency loss in the long wavelength region are ascribed to the insufficient charge collection in the absorber far from the p-n junction. As indicated by XRD results, the absorber layer has unfavorable (hk0) orientation which considerably limits the charge transport through the film. EQE measurements were performed under reverse bias condition by applying a negative voltage of -1V (which enlarges the junction width) and the results are shown by the dotted line in fig. 3 (a). The EQE was found to improve significantly in the long wavelength region (600-900 nm) for all the devices, which indicates a limited collection efficiency in the long wavelength region.

The reverse biased EQE spectrum clearly indicates that all solar cells suffered poor charge collection as mentioned previously. One of the reason for this is unfavorable crystallographic orientation of the absorber layers. A small difference was observed for the EQE spectrum collected at the 0V and -1V for the absorber grown at 320 °C. Whereas the charge carrier collection was found to be worst for the devices fabricated with the absorber annealed at 350 and 380 °C. This observation confirms the observed low J_{sc} for these devices in comparison to the cell completed with the absorber annealed at 320 °C.

Optical band gap (E_g) values were calculated from the EQE spectra. $(\ln(1\text{-EQE}))^2$ vs. hν was plotted and the straight line region was fitted to extract the optical band gap (E_g) values. No significant changes in the band gap value was observed for different annealing treatments. E_g ~ 1.3 eV was observed for all the absorbers which is in good agreement with values mentioned in literature[8,9].

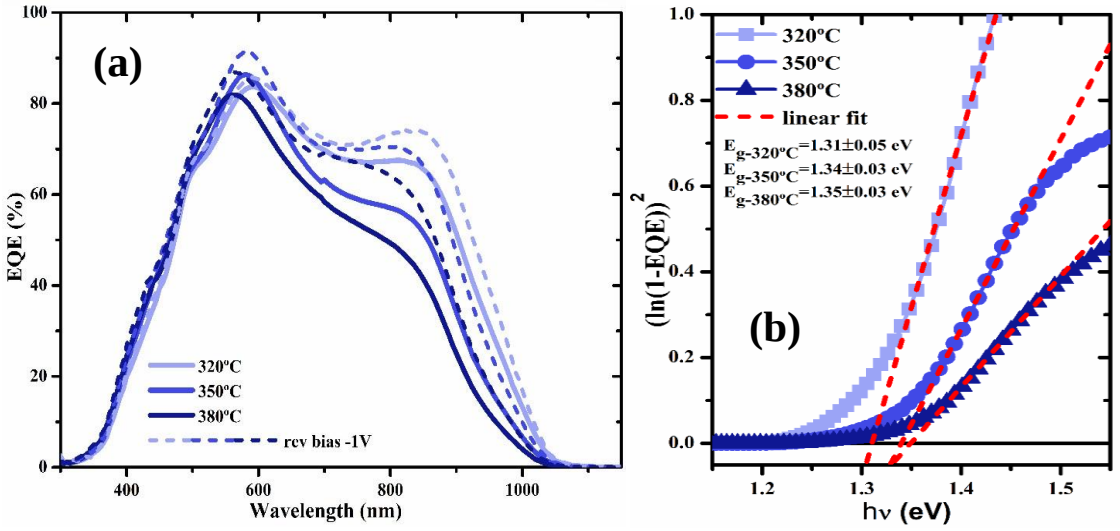

Fig. 4(a) EQE spectra for the completed solar cell devices at 0V and -1V. (b) Band gap values for the Sb_2Se_3 absorber calculated from EQE.

C-V Spectroscopy Study:

To further investigate the physics of defects in semiconductors, admittance spectroscopy based methods are widely employed. DLCP and capacitance-voltage (C-V) are two of the important methods utilized frequently. In this study we have utilized C-V measurements to measure the doping concentration and width of the space charge region.

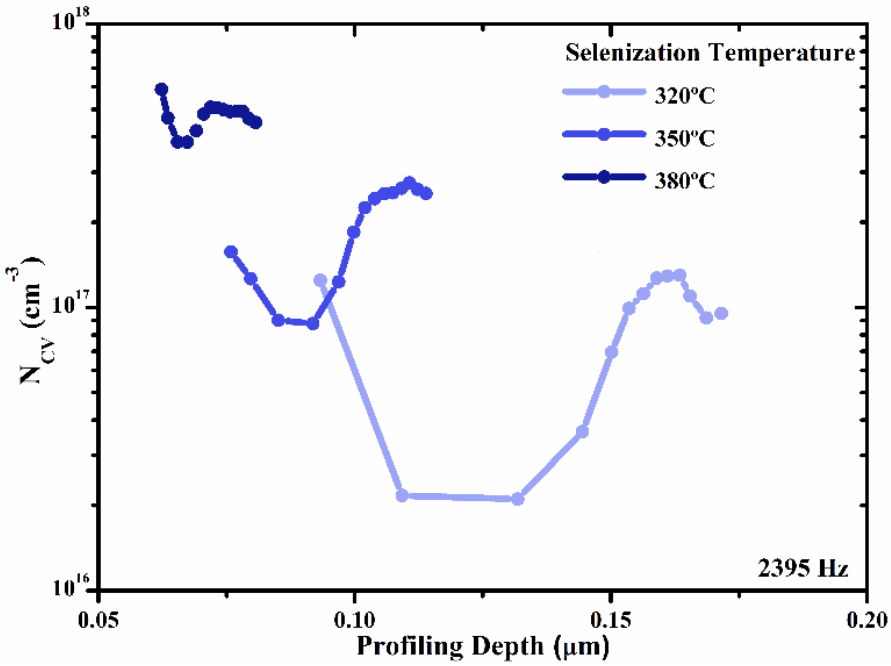

Fig. 5 C-V depth profiling of the Sb_2Se_3 thin film solar cells fabricated using the films grown at the substrate temperature of 320 °C and annealed at various temperature.

The carrier density vs. profiling depth plot for the Sb_2Se_3 solar cells obtained from the C-V measurements is shown in fig. 5. C-V measurements were performed at 0V bias and AC frequency of 2 kHz. The trend of increasing doping concentration with increase of the RTA temperature is clearly evident from the figure. Width of the space charge region (SCR) and doping concentration values (N_{cv}) are extracted from the C-V data and values are mentioned in table 2 along with the various device parameter values. The N_{cv} for all the annealed samples was found to be ~ 10^{16}-10^{17} cm^{-3}, whereas baseline carrier concentration of 10^{13} has been reported for the undoped samples for perfect stoichiometry previously[21]. A relatively high N_{cv} values relates to the effect of RTA temperature on the defect properties of the absorber. As mentioned earlier, as grown films were Se poor in stoichiometry leading to formation of V_{se}, which are detrimental for the device performance and hence resulting in non-functional solar cell devices. We hypothesize

that post selenization of absorber has increased the Se concentration in the absorber leading to formation shallow acceptor defect Se_{Sb}. Formation of these antisite defects modifies the carrier concentration of the absorber and improves the p-type conductivity of the absorber. In this study though, the thin films have a dominant unfavourable (hk0) orientation, high concentration of acceptor defects could have led to the observed device efficiency values. A high hole concentration of 2×10^{16} cm^{-3} with SCR width of 132 nm was observed for the films annealed at 320 °C. This supports the relatively high J_{sc} (21.9 mA/cm^{-2}) and low difference between the EQE spectrum collected under normal and reverse biased condition. Whereas on further increasing the selenization temperature carrier concentration increased apparently leading to shrinkage of SCR. N_{cv} of 9×10^{16} cm^{-3} with SCR width of 92 nm were obtained for the absorber annealed at temperature of 350 °C. A significant difference in the EQE measurement under normal and biased condition confirms this observation. When the measurement was performed under normal conditions due to the excess carrier concentration and narrow SCR high rate of recombination is expected. This could have resulted in the drop in the J_{sc} values for these devices. Similar kind of observation was made for the absorbers annealed at 380 °C. C-V results for these devices has shown highest N_{cv} value of $\sim 4 \times 10^{17}$ cm^{-3} with very narrow SCR of width 67 nm. This could be the possible reason behind the poor performance of the devices completed with the absorber annealed at higher temperature. Here it's worth mentioning that observed increase in the carrier concentration post selenization can be due to the formation of Se_{Sb} antisites. Now these defects act as shallow acceptor and hence have minimal or negligible impact on the fermi level.

Conclusion:

This study highlights the importance of the stoichiometry and particularly of the Se content in the absorber layer for achieving a functional Sb_2Se_3 solar cell devices. Sb_2Se_3 thin films with prominent (120) orientation were grown by e-beam evaporation from single source. Post deposition heat treatment under Se presence had a profound impact on the stoichiometry as well as performance of the solar cells. Even though the absorber had an (hk0) orientation, different from the commonly reported (hk1) orientation, an efficiency of 4.34% was still observed for the devices completed in substrate configuration using absorber annealed at 350 °C; this value is the highest reported for this crystalline orientation of the compound. The capacitance voltage analysis of the devices reveals significant changes in the defect/carrier concentration when increasing the selenization temperature. The possible formation of the Se_{Sb} antisite defect under selenium rich composition can be hypothesized, driving the carrier concentration up to ~ 10^{16}-10^{17} cm^{-3} and resulting in a significant increase in the conductivity of the absorber and performance of the solar cells. In addition, a passivation of the grain boundaries in the absorber post selenization is observed, which could also be one of the contributing elements towards improving the efficiency of the solar cells. Hence, it can be concluded that along with the crystallographic orientation, a good control of the defects and the stoichiometry of the absorber also has a vital role to play in deciding the performance of the Sb_2Se_3 solar cell devices.

Acknowledgements:

This project has received funding from the European Union's Horizon 2020 research and innovation programme under the Marie Skłodowska-Curie grant agreement No 712949 (TECNIOspring PLUS) and the Government of Catalonia's Agency for Business Competitiveness(ACCIÓ). This research was also supported by the Spanish Ministry of Science, Innovation and Universities under the WINCOST (ENE2016-80788-C5-1-R) project, and by the European Regional Development Funds (ERDF, FEDER Programa Competitivitat de Catalunya

2007-2013). Authors from IREC and the University of Barcelona belong to the SEMS (Solar Energy and Materials Systems) Consolidated Research Group of the 'Generalitat de Catalunya' (Ref. 2017 SGR 862). Ministry of New and Renewable Energy (MNRE) is very well acknowledged for funding the research activities at SRM IST through the project "Development of Lithium Ion Batteries and Computational Studies for Solar Absorber Layers, (Grant No. 31/03/2014-15/PVSE-R&D).

References:

[1] P. Sinsermsuksakul, K. Hartman, S. Bok Kim, J. Heo, L. Sun, H. Hejin Park, R. Chakraborty, T. Buonassisi, R.G. Gordon, Enhancing the efficiency of SnS solar cells via band-offset engineering with a zinc oxysulfide buffer layer, Appl. Phys. Lett. 102 (2013). doi:10.1063/1.4789855.

[2] I.Y. Ahmet, M. Guc, Y. Sánchez, M. Neuschitzer, V. Izquierdo-Roca, E. Saucedo, A.L. Johnson, Evaluation of AA-CVD deposited phase pure polymorphs of SnS for thin films solar cells, RSC Adv. 9 (2019) 14899–14909. doi:10.1039/c9ra01938c.

[3] Vidal-Fuentes, P.; Guc, M.; Alcobe, X.; Jawhari, T.; Placidi, M.; Pérez-Rodríguez, A.; Saucedo, E.; Roca, V. I. Multiwavelength Excitation Raman Scattering Study of Sb_2Se_3 Compound: Fundamental Vibrational Properties and Secondary Phases Detection. *2D Mater.* **2019**, *6* (4), 045054. https://doi.org/10.1088/2053-1583/ab4029.

[4] Y. Zhou, L. Wang, S. Chen, S. Qin, X. Liu, J. Chen, D.-J. Xue, M. Luo, Y. Cao, Y. Cheng, E.H. Sargent, J. Tang, Thin-film Sb_2Se_3 photovoltaics with oriented one-dimensional ribbons and benign grain boundaries, Nat. Photonics. 9 (2015) 409–415. doi:10.1038/nphoton.2015.78.

[5] C.N. Savory, A.M. Ganose, D.O. Scanlon, Exploring the PbS-Bi_2S_3 Series for Next Generation Energy Conversion Materials, Chem. Mater. 29 (2017) 5156–5167. doi:10.1021/acs.chemmater.7b00628.

[6] V. Steinmann, R.E. Brandt, T. Buonassisi, Non-cubic solar cell materials, Nat. Publ. Gr. 9 (2015) 355–357. doi:10.1038/nphoton.2015.85.

[7] Z. Li, X. Liang, G. Li, H. Liu, H. Zhang, J. Guo, J. Chen, K. Shen, X. San, W. Yu, R.E.I. Schropp, Y. Mai, 9.2%-Efficient Core-Shell Structured Antimony Selenide Nanorod Array Solar Cells, Nat. Commun. 10 (2019) 1–9. doi:10.1038/s41467-018-07903-6.

[8] K. Zeng, D.-J. Xue, J. Tang, Antimony selenide thin-film solar cells, Semicond. Sci. Technol. 31 (2016) 063001. doi:10.1088/0268-1242/31/6/063001.

[9] C. Chen, D.C. Bobela, Y. Yang, S. Lu, K. Zeng, C. Ge, B. Yang, L. Gao, Y. Zhao, M.C. Beard, J. Tang, Characterization of basic physical properties of Sb_2Se_3 and its relevance for photovoltaics, 3 (2017). doi:10.1007/s12200-017-0702-z.

[10] X. Liu, J. Chen, M. Luo, M. Leng, Z. Xia, Y. Zhou, S. Qin, D.J. Xue, L. Lv, H. Huang, D. Niu, J. Tang, Thermal evaporation and characterization of Sb_2Se_3 thin film for substrate Sb_2Se_3/CdS solar cells, ACS Appl. Mater. Interfaces. 6 (2014) 10687–10695. doi:10.1021/am502427s.

[11] Y. Zhou, M. Leng, Z. Xia, J. Zhong, H. Song, X. Liu, B. Yang, Solution-Processed Antimony Selenide Heterojunction Solar Cells, (2014) 1–8. doi:10.1002/aenm.201301846.

[12] L. Wang, M. Luo, S. Qin, X. Liu, J. Chen, B. Yang, M. Leng, D. Xue, Y. Zhou, L. Wang, M. Luo, S. Qin, X. Liu, J. Chen, B. Yang, M. Leng, D. Xue, Y. Zhou, L. Gao, H. Song, Ambient $CdCl_2$ treatment on CdS buffer layer for improved performance of Sb_2Se_3 thin film photovoltaics, 143902 (2015). doi:10.1063/1.4932544.

[13] X. Liu, C. Chen, L. Wang, J. Zhong, M. Luo, J. Chen, D. Xue, Improving the performance of Sb_2Se_3 thin fi lm solar cells over 4 % by controlled addition of oxygen during film deposition, (2015) 1828–1836. doi:10.1002/pip.

[14] M. Leng, M. Luo, C. Chen, S. Qin, J. Chen, J. Zhong, J. Tang, Selenization of Sb_2Se_3 absorber layer: An efficient step to improve device performance of CdS/Sb_2Se_3 solar cells, Appl. Phys. Lett. 105 (2014). doi:10.1063/1.4894170.

[15] C. Yuan, L. Zhang, W. Liu, C. Zhu, Rapid thermal process to fabricate Sb_2Se_3 thin film for solar cell application, Sol. Energy. 137 (2016) 256–260. doi:10.1016/j.solener.2016.08.020.

[16] Z. Li, X. Chen, H. Zhu, J. Chen, Y. Guo, C. Zhang, W. Zhang, X. Niu, Y. Mai, Sb_2Se_3 thin fi lm solar cells in substrate configuration and the back contact selenization, 161 (2017) 190–196. doi:10.1016/j.solmat.2016.11.033.

[17] X. Wen, Y. He, C. Chen, X. Liu, B. Yang, Magnetron sputtered ZnO buffer layer for Sb_2Se_3 thin film solar cells, 172 (2017) 74–81. doi:10.1016/j.solmat.2017.07.014.

[18] C. Chen, D.C. Bobela, Y. Yang, S. Lu, K. Zeng, C. Ge, B. Yang, L. Gao, Y. Zhao, M.C. Beard, J. Tang, Characterization of basic physical properties of Sb_2Se_3 and its relevance

for photovoltaics, Front. Optoelectron. 10 (2017) 18–30. doi:10.1007/s12200-017-0702-z.

[19] C. Chen, K. Li, S. Chen, L. Wang, Efficiency Improvement of Sb_2Se_3 Solar Cell via Grain Boundary Inversion, (2018). doi:10.1021/acsenergylett.8b01456.

[20] G. Li, Z. Li, X. Liang, C. Guo, K. Shen, Y. Mai, Improvement in Sb_2Se_3 solar cell efficiency through band alignment engineering at the buffer/absorber interface, ACS Appl. Mater. Interfaces. 11 (2018) 828–834. doi:10.1021/acsami.8b17611.

[21] X. Liu, X. Xiao, Y. Yang, D. Xue, D. Li, C. Chen, S. Lu, L. Gao, Y. He, M.C. Beard, G. Wang, S. Chen, Enhanced Sb_2Se_3 solar cell performance through theory-guided defect control, (2017). doi:10.1002/pip.2900.

[22] M. Huang, P. Xu, D. Han, J. Tang, S. Chen, Complicated and Unconventional Defect Properties of the Quasi- One-Dimensional Photovoltaic Semiconductor Sb_2Se_3, ACS Appl. Mater. Interfaces. 11 (2019) 15564–15572. doi:10.1021/acsami.9b01220.

[23] Z. Li, H. Zhu, Y. Guo, X. Niu, X. Chen, C. Zhang, W. Zhang, X. Liang, D. Zhou, J. Chen, Y. Mai, Efficiency enhancement of Sb_2Se_3 thin-film solar cells by the co-evaporation of Se and Sb_2Se_3, Appl. Phys. Express. 9 (2016) 052302. doi:10.7567/APEX.9.052302.

[24] Savory, Christopher N., and David O. Scanlon, The complex defect chemistry of antimony selenide. *Journal of Materials Chemistry A* 7, no. 17 (2019): 10739-10744. doi:10.1039/C9TA02022E.

[25] K.J. Tiwari, M. Ren, S. Kamalakar, T. Osipowicz, Mechanochemical bulk synthesis and e-beam growth of thin fi lms of Sb_2Se_3 photovoltaic absorber, Sol. Energy. 160 (2018) 56–63. doi:10.1016/j.solener.2017.11.074.

[26] Neuschitzer, Markus, Moises Espindola Rodriguez, Maxim Guc, Jose A. Marquez, Sergio Giraldo, Ian Forbes, Alejandro Perez-Rodriguez, and Edgardo Saucedo, Revealing the beneficial effects of Ge doping on $Cu_2ZnSnSe_4$ thin film solar cells, *Journal of Materials Chemistry A* 6, no. 25 (2018): 11759-11772.

Appendix:

Supplementary Information File:

- **Fig. S1 Trend for the obtained Sb and Se atomic percentage values with respect to the annealing temperature.**

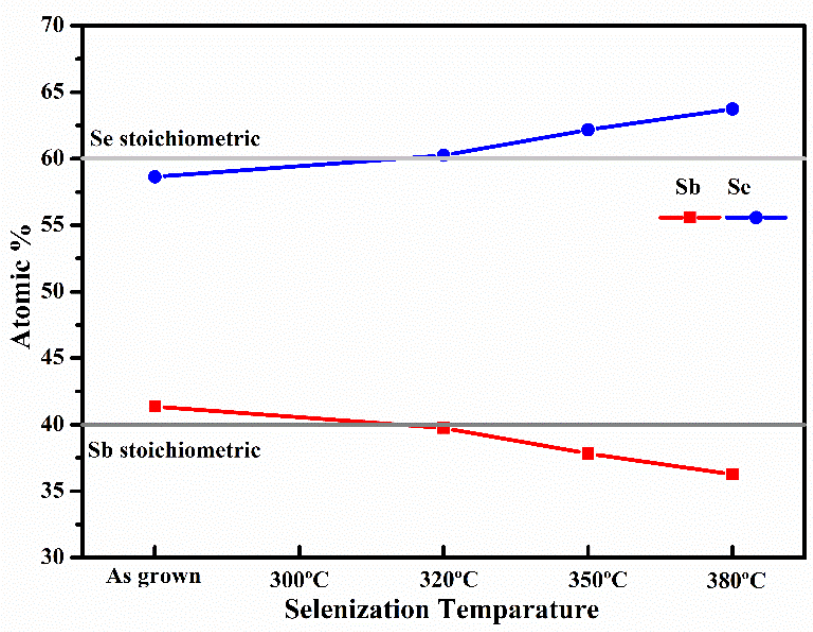

- **Fig. S2 Fitted dark J-V curves for the Sb_2Se_3 solar cells.**

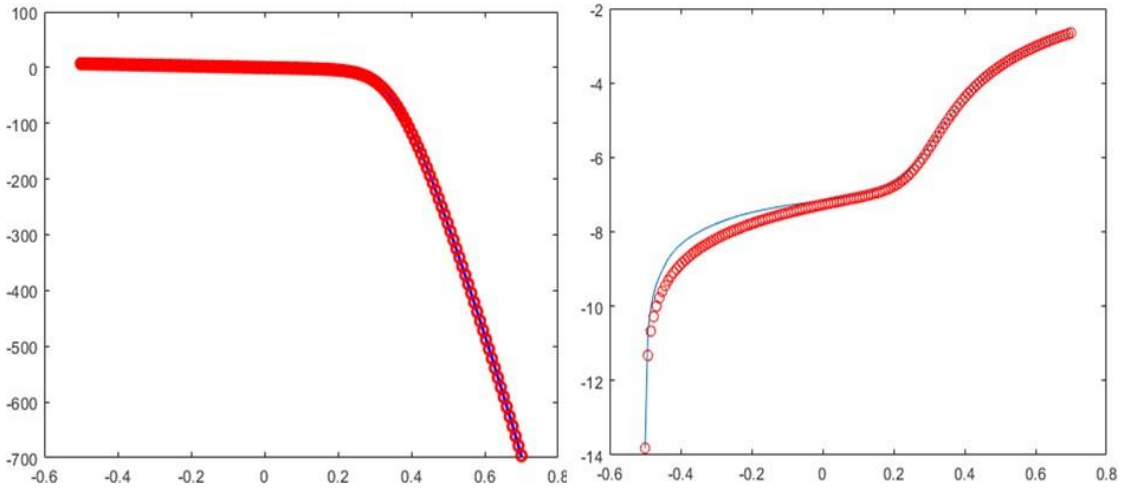

Fig. S2 (a) For solar cells completed with absorber layer annealed at 320 °C.

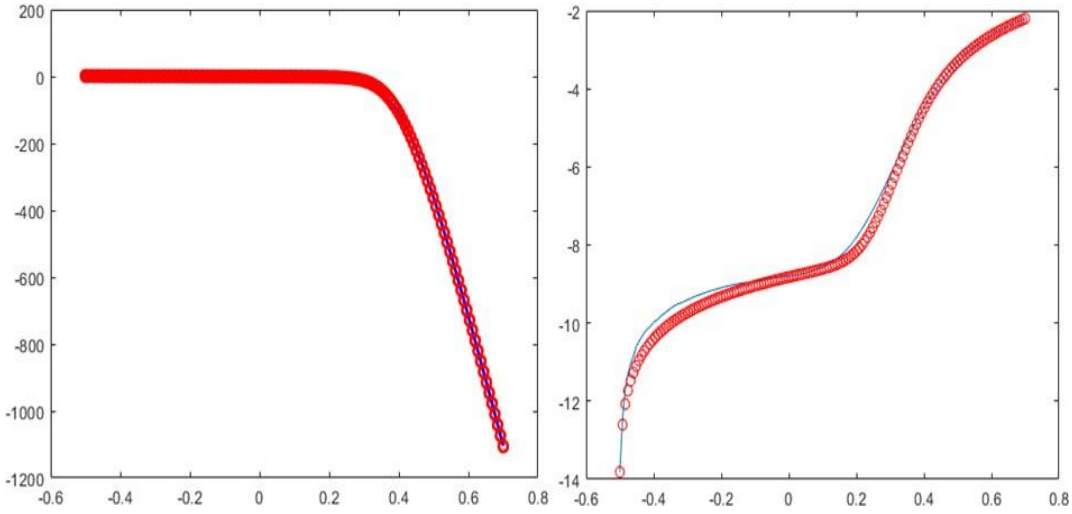

Fig. S2(b) For solar cells completed with absorber layer annealed at 350 °C.

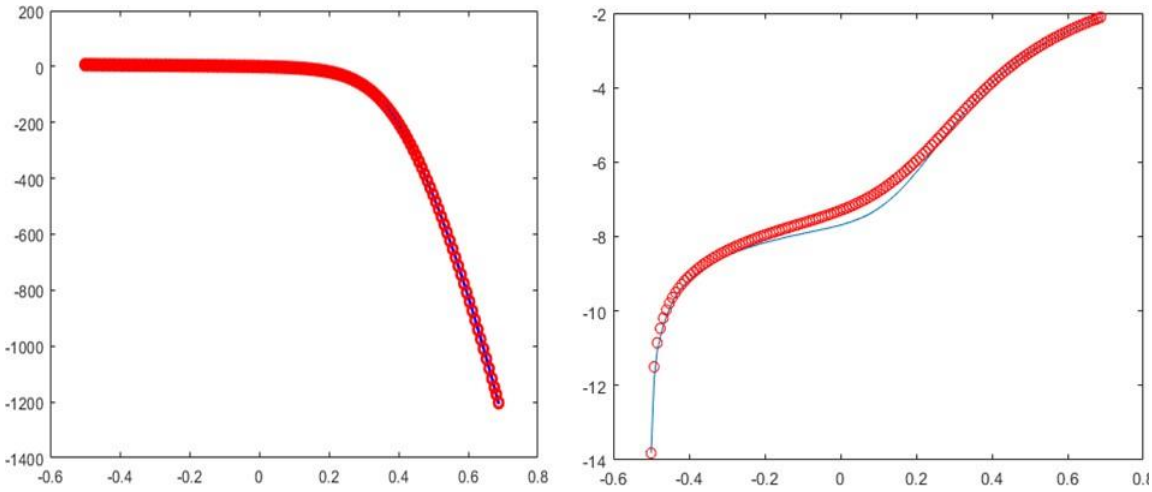

Fig. S2 (c) For solar cells completed with absorber layer annealed at 380 °C.

- **Table S1. Comparison of the efficiency values reported in the literature for the Sb_2Se_3 solar cells fabricated in the substrate configuration with the results reported in this study.**

Sl.No.	Device Structure	Film Orientation	V_{oc} (mV)	J_{sc} (mA/cm^2)	FF (%)	η(%)	Ref.
1.	Glass/Mo/$MoSe_2$/NA-Sb_2Se_3/TiO2/CdS/ZnO/Al:ZnO	(211)	400	32.58	70.3	9.2	[1]
2.	Glass/Mo/TF-Sb_2Se_3/CdS/ZnO/Al:ZnO	(211)	368	24.87	49.53	4.53	[1]
3.	Glass/Mo/Sb_2Se_3/CdZnS/ZnO/	(221)	403	25.69	64.78	6.71	[2]
4.	Glass/Mo/Sb_2Se_3/CdS/ZnO	(221)	383	24.33	54.52	5.08	[2]
5.	Glass/Mo/$MoSe_2$/Sb_2Se_3/CdS/ZnO/	(221)	427	17.11	58.15	4.25	[3]
6.	Glass/Mo/Sb_2Se_3/CdS/ZnO	(221)	398	15.96	48.26	3.07	[3]
7.	**Glass/Mo/Sb_2Se_3/CdS/ZnO**	**(120)**	**386**	**19.8**	**56.7**	**4.34**	**This work**

NA – Nano rod array of Sb_2Se_3

TF- Thin films of Sb_2Se_3

References:

(1) Li, Z.; Liang, X.; Li, G.; Liu, H.; Zhang, H.; Guo, J.; Chen, J.; Shen, K.; San, X.; Yu, W.; et al. 9.2%-Efficient Core-Shell Structured Antimony Selenide Nanorod Array Solar Cells. *Nat. Commun.* **2019**, *10* (1), 1–9. https://doi.org/10.1038/s41467-018-07903-6.

(2) Li, G.; Li, Z.; Liang, X.; Guo, C.; Shen, K.; Mai, Y. Improvement in Sb_2Se_3 Solar Cell E Ffi Ciency through Band Alignment Engineering at the Buffer / Absorber Interface. *ACS Appl. Mater. Interfaces* **2018**, *11*, 828–834. https://doi.org/10.1021/acsami.8b17611.

(3) Li, Z.; Chen, X.; Zhu, H.; Chen, J.; Guo, Y.; Zhang, C.; Zhang, W.; Niu, X.; Mai, Y. Solar Energy Materials & Solar Cells Sb_2Se_3 Thin Film Solar Cells in Substrate Con Fi Guration and the Back Contact Selenization. **2017**, *161* (July 2016), 190–196. https://doi.org/10.1016/j.solmat.2016.11.033.